IMPACT
International Microsystems , Packaging,
Assembly and Circuits Technology conference

Structural Analysis and Static Responses of Electrostatic Actuators for 3-DOF Micromanipulators in Phonomicrosurgery

Eakkachai Pengwang[1,2], Kanty Rabenorosoa[1], Micky Rakotondrabe[1], and Nicolas Andreff [1]

[1]FEMTO-ST Institute UMR CNRS 6174-UFC/ENSMM/UTBM,
Automatic Control and Micro-Mechatronic Systems Department (AS2M), Besançon, 25000 France.

[2]Institute of Field Robotics, King Mongkut's University of Technology Thonburi
126 Pracha-Utid Road, Bangmod, Thrung Kru, Bangkok 10140 Thailand

eakkachai@fibo.kmutt.ac.th

While the searching for electrostatic actuators with large displacements is going on, this paper will demonstrate the parameters that influence the performances of linear electrostatic actuators. A comparison of theoretical calculations and experimental results for linear electrostatic actuators will also be presented for phonomicro-surgery. Theoretically, transverse displacement of electrostatic comb drive depends on supplied voltage, pull-in voltage, and length of spring suspension. In this study, two types of spring suspension (single beams and double-folded beams) are studied for different behaviors of linear electrostatic actuators. Normally, the folded-beam are implemented with the guilded-axis along at the center. There are still contradictions about the deflection of the single beam suspension and the folded-beam. Engineers and scientists predicted the deformations for their own designs. Some results show that the single beam can provide higher deformation, while the other reported the result for both design are relevant or higher. Calculations of stiffness and allowable transverse displacement are also compared to the simulation results among different types. The calculations are used for designing the performances of electrostatic actuators with a fit-curve for different parameters. Then, the experimental results indicate characteristics of linear electrostatic actuators for different suspension designs and different parameters. Next, these electrostatic actuators will be implemented for a 3-DOF (tip-tilt-piston) micro-mirror in phonomicrosurgery by using a micro-assembly approach with marker and assembly block to place three electrostatic comb-drives in the precise position. With this development, MEMS-based micro-mirror designs can enhance capability of biomedical apparatus that require high speed, low power consumption, and high reliability.

Keywords: Electrostatic actuators, Microassembly, Micromirrors, Manipulator dynamics, Micromanipulators

INTRODUCTION

In the past decades, several forms of micromirrors have been investigated for optical applications and laser phonomicrosurgery, for example, electrostatic actuators [1-8], electrothermal actuators [9-12], piezoelectric actuators [13-14], electromagnetic actuators [15], acoustic actuators, pneumatics actuators, and shape memory alloys [16]. Electrostatic actuators are implemented in many applications such as accelerometers, scanning mirrors, photonics, televisions, and projectors. The limitation of electrostatic actuators can be a pull-in voltage and high driving voltage on the order of 100 V. For medical application, micro scanning mirror with electrostatic actuators are also investigated widely because they are fast response, consume low power, and yield large scanning angle. For example, the MicroRALP project that investigates on micromanipulator with a large scanning range for a laser phonomicrosurgery [17-18]. This project aims to design and analysis of micro robots are investigated with suitable actuators and mechanism to create a tip-tilt-piston micro-mirror.

In general, linear electrostatic actuators are implemented in various applications. Different geometries, shapes of comb, flexure hinges, spring suspension, and materials are investigated for a high range of motion, faster speed, and high dynamic response. Linear electrostatic comb-drives are implemented for several scanning micromirrors with in-plane motions [1-8]. The range of motion is up to 30 µm for two-axis stages. In general, high-aspect-ratio etching such as deep-reactive-ion-etching (DRIE) methods on SOI wafers, is a key for fabrication for these electrostatic actuators. These methods can be used for both creating the structures of linear comb-drives and releasing them from the substrates. Another approach is to implement a compliant actuation with high suspension stiffness for six-DOFs precision manipulator [19]. This device is designed with the micro- assembly of electrostatic actuators with submicron platform. However, the maximum strokes of these actuators are only 20 µm displacement that results to ±10 µm displacement at the end-effector. Another method to combine linear electrostatic actuators with parallel-plate actuators for 3-axis nanopositioning MEMS stage was reported by Liu et al. [10]. By using four sets of comb-drive for in-plane motion and parallel-electrodes for out-of-plane motion, the device was reported for a displacement of ±12.5 µm in the X and Y directions at 30 V and ±3.5 µm in the Z direction at 14.8 V. Moreover, the design of linear comb actuator can be implemented for angular motions of scanning micromirrors.

In this paper, analysis of parameters for beam suspension will be focused. Two types of beam suspension (single beam suspension and modified of folded-beam suspension) are presented and examined in detailed. The half-model of single beam suspension is shown in Fig. 1. In this design, four linkages are used to fix the entire structure of movable comb. The length of the beam is 1500 µm for all four beams. Next, the modified of folded-beam in this study is shown in Fig. 2. Normally, the folded-beam are implemented with the guilded axis along at the center. The length of the bottom beams is 1500 µm, but the length of the top beams is 1050 µm so that the fixed base can be located next to the center area. Both of designs are used in MEMS and micro devices, but there are still contradictions about the deflection of the single beam suspension and the folded-beam. Engineers and scientists predicted the deformations for their own designs. Some results showed that the single beam can provide higher deformation, while the other reported the result from a folded beam suspension is higher. In this paper, the experimental results and simulation will be analyzed and compared.

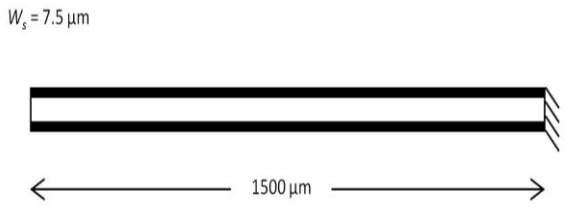

FIGURE 1. SCHEMATIC OF SINGLE BEAM SUSPENSION

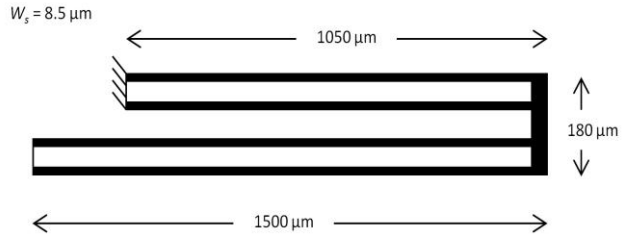

FIGURE 2. SCHEMATIC OF DOUBLE-FOLDED BEAM SUSPENSION

THEORETICAL CALCULATIONS

The principle of electrostatic actuator is the static charge phenomena in each pair of adjacent comb finger. The actuator can generate electrostatic force by the change of capacitance. In order to stabilize the comb-drive, the mechanical stiffness of the comb drive is connected to the spring and the anchor. However, the spring stiffness of each design and batch are different. In this section, two designs of beam suspension; single beam with four legs (Design A) and folded beam with two anchors and two legs for each side (Design B) will be examined. In common, the electrostatic force (F_{comb}) generated by comb fingers depends on gap between electrodes (d), thickness of comb finger (t), supplied voltage (V), permittivity of the media (ε) , and number of pairs of comb fingers (n). The deflection (δ_{comb}) of comb-drive actuators connected to beam suspensions is depicted with Equation 1.

$$\delta_{comb} = \frac{F_{comb}}{k_{eff}} = n \cdot \frac{\varepsilon \cdot t \cdot V^2}{d} \cdot \frac{L^3}{4 \cdot E_{spring} \cdot h \cdot b^3} \quad [1]$$

where L is the length of the beam suspension, E is the Young's modulus of the material, h is the height of the beam suspension, and b is the width of the beam suspension. It is also noted that the height of the device is not influenced on the defection if the thickness of the beam suspension (h) and comb fingers (t) are the same. Moreover, the number of pairs of comb fingers (n) depends on the width of comb finger and the gap between electrodes as well.

For a modified folded-beam suspension, the calculation for spring stiffness (k_{eff}) is different than the single-beam suspension. Two models are formulated as shown in Equation 2-3 and the averaged values are used for the analysis.

$$\frac{1}{k_e} = \frac{1}{Et}\left(\frac{L^3}{2w^3} + \frac{6(1+\mu)L}{5w} + \frac{L_r}{2w_r} + \frac{3L^2L_r}{2w_r^3}\right) \quad [2]$$

$$\frac{1}{k_e} = \frac{1}{Et}\left(\frac{L^3}{2w^3} + \frac{3(1+\mu)L}{5w} + \frac{L_{c2}}{4w_{c2}} - \frac{3LL_{c2}^2}{4w_{c2}^3}\right) \quad [3]$$

From the calculations with designed values, the double-folded spring will have lower stiffness in actuating direction. The result of stiffness is about 0.75 for the system shown in Fig. 2 (this is approximately 77% of the values for single spring system shown in Fig. 1). As a result, the deflection of the electrostatic actuators with double-folded beam could be improved by 30% compared to the single spring system.

Moreover, side instability voltages are considered in this analysis as well. The characteristics of electrostatic actuators are resulted from the capacitance values between two adjacent fingers, hence the spring suspension can snap in to the side at different values. From the calculation of capacitance value, the maximum displacement can occur at this point of side-instability voltage. The calculation of side-instability can be explained in Equation 4. From this equations, the double-folded beam are expected to have lower values for side-instability voltage compared to the single beam suspension.

$$V_{SI}^2 = \frac{d^2 k_y}{2\epsilon_0 bn}\left(\sqrt{2\frac{k_x}{k_y} + \frac{y_0^2}{d^2}} - \frac{y_0}{d}\right) \quad [4]$$

In this paper, several patterns of electrostatic actuators will be examined, for example, downward motion (Configuration 1), upward motions (Configuration 2), two-set of downward motion in series (Configuration 3), bi-directional motions (Configuration 4), and 3-set of downward motion (Configuration 5). The notation of each pattern is summarized in Table I. Nevertheless, the finger width and finger gap is also investigated for characterizations of electrostatic actuators. The values of finger width and finger gap also affect the number of comb in the same length as shown in Table II.

TABLE I: PARAMETER FOR ELECTROSTATIC ACTUATORS

Design A (single beam)		**Design B (double-folded beam)**	
A1	Downward	B1	Downward
A2	Upward	B2	Upward
A3	2-set	B3	2-set
A4	Bi-direction	B4	Bi-direction
A5	3-set	B5	3-set

TABLE II: DESIGN VALUES AND RESULTS FROM FABRICATION PROCESSES

Batch Number	Designed Parameters	Fabricated Devices
I	4µm finger/ 4µm gap (180 pairs)	2.2µm finger/ 5.8µm gap
II	5µm finger/ 5µm gap (150 pairs)	3.3µm finger/ 6.7µm gap
III	12µm finger/ 3µm gap (100 pairs)	9.0µm finger/ 6.0µm gap

For 100 pairs of electrostatic actuators with a thickness of 15 µm and the gap of 6 µm, the electrostatic force at 100 V is 20.6 µN. For design A (four single spring suspensions), the stiffness of systems is about 0.97 N/m. The lateral motion of electrostatic comb-drive is

21.3 µm. With the same actuating force, design B (four double-folded spring suspensions) can generate about 28.68 µm in displacement with a stiffness of systems about 0.72 N/m. Similarly, the required voltage can be predicted for different configurations as shown in Figure 4. In this graph, the required voltage is calculated for Design A with a displacement of 50 µm. Among different configurations, BatchI (5.8 µm gap and 2.2 µm finger) used a minimum operating voltage of 50 V for 50 µm movement. Moreover, important parameter that can affect the side-instability and displacement of the electrostatic actuators are number of pairs of comb fingers. More pairs will lower the required voltage for the same displacement of actuators. However, more pairs will increase the performances of the actuators as shown in Figure 4. Increasing numbers of finger pairs will increase values of electrostatic forces as shown in Equation 1. From the calculations, if two rows and three rows of comb-actuators are used, the actuating displacement will increase to 2 times and 3 times respectively. Considering the required voltages for the same displacement, two rows and three rows of comb-actuators can reduce the required voltage by 30% and 40% of the values for one-row design.

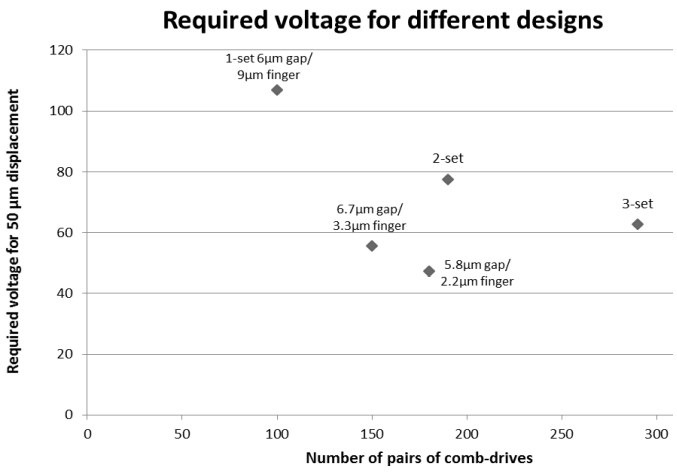

FIGURE 4. CALCULATION RESULTS FOR VOLTAGE REQUIRED FOR 50-MICROMETER-DISPLACEMENT OF ELECTROSTATIC ACTUATORS DESIGN B

Another simulation results show the effect of each parameter; width of spring (shown in Figure 5) and gap of electrostatic finger (shown in Figure 6). It can be observed that the width of spring is the most important parameter. When the width of the spring suspension is smaller, the generating displacement of electrostatic actuator increases. Other parameters, such as the finger width, finger gap, and thickness of electrostatic actuators can affect the performances of electrostatic actuators as well.

Moreover, Finite Element Analysis (FEA) are simulated for the static displacements of electrostatic actuators. The simulation is performed by COMSOL® Finite Element Analysis (FEA) software. An example of result is showed in Figure 7. In this example, the half model of electrostatic actuators with single beam suspension are tested with 100 V. The linear electrostatic in design A can move up to 11.2 µm when it is actuated at 100 V. Hence, these results are corresponded to the theoretical calculations in the previous discussions.

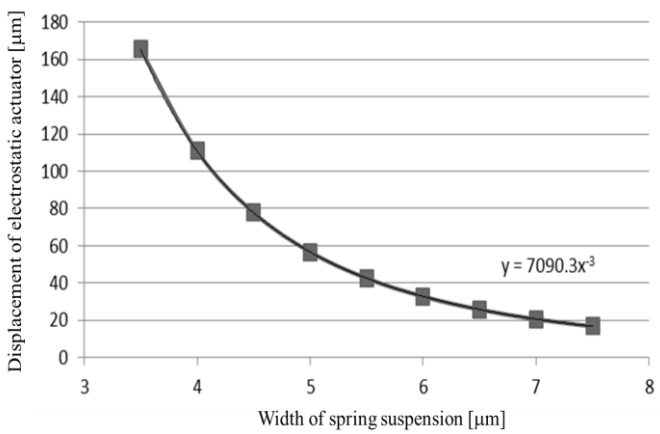

FIGURE 5. DATA FITTING FOR ELECTROSTATIC DISPLACEMENT WITH DIFFERENT WIDTH OF SPRING SUSPENSION

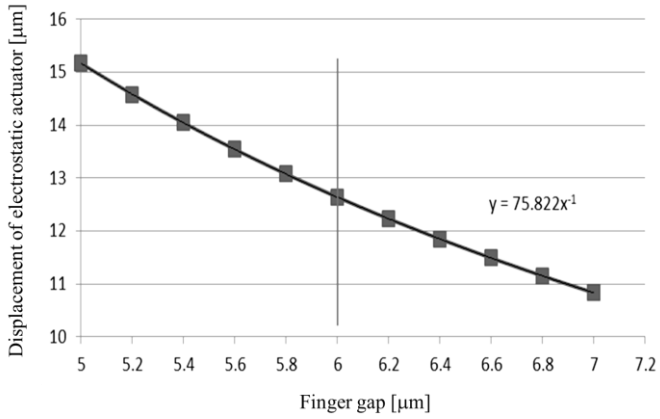

FIGURE 6. DATA FITTING FOR ELECTROSTATIC DISPLACEMENT WITH DIFFERENT GAP BETWEEN ELECTROSTATIC FINGERS

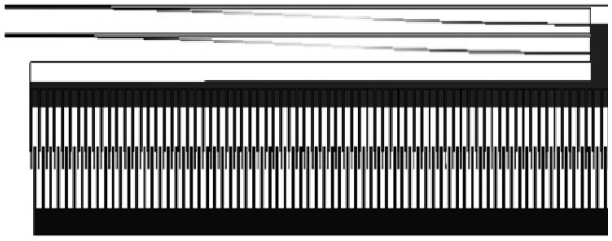

FIGURE 7. COMSOL® SIMULATION RESULT FOR SINGLE BEAM SUSPENSION (DESIGN A)

MICROFABRICATION PROCESS

The microfabrication process of the linear electrostatic actuator and mirror is conventional thin-film lithography process and dry etching. SOI wafer with device layer of 15 µm on a 500-µm-thick handle layer is patterned for electrical pads and structure for electrostatic comb drive. Chrome and gold is deposited and patterned for electrical pad by photolithography and wet etchant. Next, the mask for structure is patterned by photoresist and deep reactive-ion-etching (DRIE) on the device layer. The high-aspect-ratio structure is created by a deep-reactive-ion-etching (DRIE) process. The alignment mark on the front side is then used to align the backside

etching mask on the handling layer. The process of reactive-ion-etching is used for etching the backside. Then, the wafer is immersed in vapor hydrofluoric acid to remove the oxide layer. Last, all of phororesist mask is removed to complete the electrostatic actuators with cantilever.

TESTING RESULTS

The static tests of electrostatic actuators are performed with the Polytec® Micro System Analyzer (MSA-500 Model, Chatillon, France) and the Planar Motion Analyzer software (PMA Version 2.6). Although there are different values for measuring methods, several samples of electrostatic actuators are performed and the average values are used. The testing results shown that the pull-in voltage is an important parameter that can affect the performance of electrostatic actuator as shown in Table III. For the singer beam suspension, the design with downward motion can move about 20 μm at 200 V and still not reach the pull-in voltage. While the multiply sets of row (Configuration 2, 3, and 5) can move about the same displacement, but the actuators reach the pull-in conditions. For Design B (folded beam suspension), the maximum displacement occurs at configuration B1 for a displacement of 50 μm at 80 V. The upward motion (B2), two-row can reach about the same displacements. The side instability still limit the performance for the bi-direction (B4) and three-row (B5) configuration. The testing results also show that the folded-beam suspension has a better displacement and lower side instability voltage than the single-beam suspension in all configuration.

TABLE III: TESTING RESULTS FOR PERFORMANCES OF ELECTROSTATIC ACTUATORS FOR DIFFERENT DESIGNS

Design	Maximum static displacement [μm]
A1	19.42 μm at 200V *(not pull in yet)*
A2	19.92 μm at 150V
A3	19.43 μm at 116 V
A4	12.54 μm at 200 V *(not pull in yet)*
A5	13.58 μm at 75 V
B1	53.69 μm at 80V
B2	51.77 μm at 120V
B3	47.15 μm at 55V
B4	36.20 μm at 60V
B5	20.82 μm at 40V

Although there are still inconclusive about the characteristics of electrostatic actuators with different comb finger and electrode gap, the testing results showed that the maximum displacement (80 μm) occurs when the comb finger is 3.3 μm and the gap between the comb fingers is 6.7 μm. The operating voltage for this case is 26 V. The comparisons between each batch (different comb finger and electrode gap) are shown in Table IV. It is noted that the performance is not improved when the gap and the finger width is smaller. One of assumptions is the values of width of spring and gap distance can be varied for different locations on wafer in microfabrication techniques. However, these testing results of electrostatic actuators and the structural analysis are verified in this paper. For the high scanning range of motion, the two-set of comb with folded beam suspension is recommended.

TABLE IV: TESTING RESULTS FOR PERFORMANCES OF ELECTROSTATIC ACTUATOR WITH DIFFERENT GAP VALUES (DOUBLE-FOLDED BEAM SUSPENSION WITH 2 SETS OF COMB)

Design	Maximum static displacement [μm]
3.3μm finger/ 6.7μm gap (280 pairs)	79.17 μm at 26V
9.0μm finger/ 6.0μm gap (190 pairs)	28.52 μm at 56V
2.2μm finger/ 5.8μm gap (340 pairs)	40.8 μm at 12V

REFERENCES

[1] K. Laszczyk, S. Bargiel, C. Gorecki, J.J. Krezel, P. Dziuban, M. Kujawinska, M. Kujawinskab, D. Callet, and S. Frank, *Sensors Actuators A*, 2010, vol. 163, pp. 255-265.

[2] D. Mukhopadhyay, J. Dong, E. Pengwang, and P. Ferreira, *Sensors Actuators A*, 2008, vol. 147, pp. 340-351.

[3] W. Jung, D. T. McCormick, J. Zhang, L. Wang, N. C. Tien, and Z. Chen, *Appl. Phys. Lett.*, 2006, vol. 88, pp. 163901.

[4] D. T. McCormick, W. Jung, Y. C. Ahn, Z. Chen, and N. C. Tien, *Proc. Solid-State Sensors, Actuators and Microsystems Conf., 2007 (TRANSDUCERS 2007)*, 2007, pp. 203-208.

[5] A. D. Aguirre, P. R. Hertz, Y. Chen, J. G. Fujimoto, W. Piyawattanametha, L. Fan, and M. C. Wu, *Opt. Express*, 2007, vol. 15, pp. 2445-2453.

[6] K. Kumar, J. C. Condit, A. McElroy, N. J. Kemp, K. Hoshino, T. E. Milner, and X. Zhang, *J. Optics A-Pure Appl. Opt.*, 2008, vol. 10, pp. 044013.

[7] K. H. Jeong and L. P. Lee, *J. Micromech. Microeng.*, 2005, vol. 15, pp. 277.

[8] J. T. W. Yeow, V. X. D. Yang, A. Chahwan, M. L. Gordon, B. Qi, I. A. Vitkin, B. C. Wilson, and A. A. Goldenberg, *Sensors Actuators A*, 2005, vol. 117, pp. 331-340.

[9] J. Singh, J. H. S. Teo, Y. Xu, C. S. Premachandran, N. Chen, R. Kotlanka, M. Olivo, and C. J. R. Sheppard, *J. Micromech. Microeng.*, 2008, vol. 18.

[10] L. Liu, L. Wu, J. Sun, E. Lin, and H. Xie, *J. Biomed. Opt.*, 2011, vol. 16, pp. 026006.

[11] J. Sun, S. Guo, L. Wu, L. Liu, S. Choe, B. S. Sorg, and H. Xie, *Opt. Express*, 2010, vol. 18, pp. 12065.

[12] U. Izhar, A. B. Izhar, and S. Tatic-Lucic, *Sensors Actuators A*, 2011, vol. 167, pp. 152-161.

[13] K. H. Koh, T. Kobayashi, J. Xie, A. Yu, and C. Lee, *J. Micromech. Microeng.*, 2011, vol. 21, pp. 075001.

[14] Y. Zhu, W. Liu, K. Jia, W. Liao, and H. Xie, *Sensors Actuators A*, 2011, vol. 167, pp. 495-501.

[15] K. H. Kim, B. H. Park, G. N. Maguluri, T. W. Lee, F. J. Rogomentich, M. G. Bancu, B. E. Bouma, J. F. de Boer, and J. J. Bernstein, *Opt. Express*, 2007, vol. 15, pp. 18130-18140.

[16] Y. Q. Fu, M. Hu, H. Du, J. Luo, A. J. Flewitt, and W. I. Milne, *Proc. Smart Materials, Nano-, and Micro-Smart Systems*, 2005, pp. 145-153.

[17] E. Pengwang, K. Rabenorosoa, M. Rakotondrabe, and N. Andreff, *Proc. Russian Bavarian Conf. on Bio-Medical Engineering (RGC2013)*, 2013.

[18] E. Pengwang, K. Rabenorosoa, M. Rakotondrabe and N. Andreff, *Proc. IEEE/ASME Int. Conf. Mechatronic and Embedded Systems and Applications (MESA)*, 2014, pp. 1-6.

[19] D. M. Brouwer, B. R. De Jong, and H. M. Soemers, *Precision Engineering*, 2010, vol. 34(2), pp. 307–319.